Chinese Chemical Letters 33 (2022) 2579–2584

Contents lists available at ScienceDirect

Chinese Chemical Letters

journal homepage: www.elsevier.com/locate/cclet

Constructing a coplanar heterojunction through enhanced π-π conjugation in g-C_3N_4 for efficient solar-driven water splitting

Zihao Chen[a], Ben Chong[a], Nathan Wells[a], Guidong Yang[a,*], Lianzhou Wang[b,*]

[a] XJTU-Oxford International Joint Laboratory for Catalysis, School of Chemical Engineering and Technology, Xi'an Jiaotong University, Xi'an 710049, China
[b] School of Chemical Engineering and Australian Institute for Bioengineering and Nanotechnology, the University of Queensland, QLD 4072, Australia

ARTICLE INFO

Article history:
Received 28 July 2021
Revised 7 August 2021
Accepted 28 August 2021
Available online 3 September 2021

Keywords:
g-C_3N_4
Charge separation
Coplanar heterojunction
Enhanced π-π conjugation
Photocatalysis

ABSTRACT

Adjusting the electronic structure of graphitic carbon nitride (g-C_3N_4) photocatalyst through π-π conjugation is an effective method to achieve efficient photogenerated carrier separation. One key challenge of π-π conjugation control is to tune the degree of such conjugation without destroying the g-C_3N_4 structure. Herein we report a conceptual design that achieves a coplanar heterojunction by enhancing the π-π conjugation *via* the doping of crystalline g-C_3N_4 using a conjugated double bond ring molecule, 1,3,5-benzenetriol, during calcination process. The selection of the dopant enables the facile creation of a unique coplanar heterojunction which not only retains the pristine network structure of g-C_3N_4, but remarkably promotes separation and transfer of photogenerated carriers through the enhanced π-conjugated endogenous electric field. As a result, the new g-C_3N_4 photocatalyst efficiently photocatalytically produces hydrogen from water under visible light irradiation with a high H_2 production rate up to 94.94 μmol/h, and a notable external quantum efficiency of 16.4% at 420 nm.

Utilization of semiconductor photocatalytic materials for solar driven environmental and energy applications such as splitting of water to produce hydrogen has attracted increasing attention [1–3]. In recent years, organic semiconductor graphitic carbon nitride (g-C_3N_4), comprised of polymerized triazine rings, has shown its promise for use as a metal free, highly photoactive, chemically and biologically inert photocatalyst, particularly for application as a hydrogen evolution reaction (HER) catalyst [4–9]. A great deal of work has been done in order to enhance the photocatalytic activity of g-C_3N_4 by element doping [10,11] or heterojunction construction [12–14], and more recently, modification of the electronic structure by introducing different aromatic molecules to adjust the π-π conjugation in g-C_3N_4 [15,16]. For organic semiconductors, since the semiconductor characteristics are determined by the delocalized π system, adjusting the degree of delocalization of its π system is an effective means to improve the semiconductor properties of g-C_3N_4 [17]. In particular, the π delocalization causes a narrowing of the band gap, thereby increasing the amount of light to be harvested by the semiconductor, improving visible-light driven photocatalytic performance. However, due to the weak driving force in the semiconductor plane, only those photogenerated charge carriers around the solid/liquid interface can be separated, and it is still inevitable that a large percentage of the charge carriers in the bulk phase will recombine, leading to a limited increase in photocatalytic efficiency [18]. The high electronegativity of nitrogen atoms in a triazine ring results in an asymmetric redistribution of electrons among the nitrogen atoms and the carbon atoms, which leads to the increase of π-deficiency in the conjugated system, thereby reducing the availability of electrons [19,20]. One solution to this problem is to introduce benzene rings into the polymer structure, which can effectively improve the degree of π electron delocalization, leading to improved conductivity, electron availability and light harvesting ability [21]. Additionally, there is a potential difference between the pristine g-C_3N_4 domains and benzene doped planar regions, which may lead to an endogenous coplanar heterojunction, enhancing the directional transportation of photogenerated carriers, therefore reducing recombination [22–26]. However, one challenge is the possible damage to the pristine network structure of g-C_3N_4 upon introducing the benzene ring into the structure [23,27], which could lead to incomplete polymerization of the -NH_2 group if the dopant precursors were selected without detailed consideration [28]. The unreacted -NH_2 groups, often defined as structure defects, act as charge trap sites in photocatalytic reactions, resulting in low photocatalytic activity [29–31]. To improve the charge separation and photocatalytic property of g-C_3N_4, it is of urgent need to design an efficient coplanar heterojunction by deliberately

* Corresponding authors.
E-mail addresses: guidongyang@xjtu.edu.cn (G. Yang), l.wang@uq.edu.au (L. Wang).

https://doi.org/10.1016/j.cclet.2021.08.118
1001-8417/

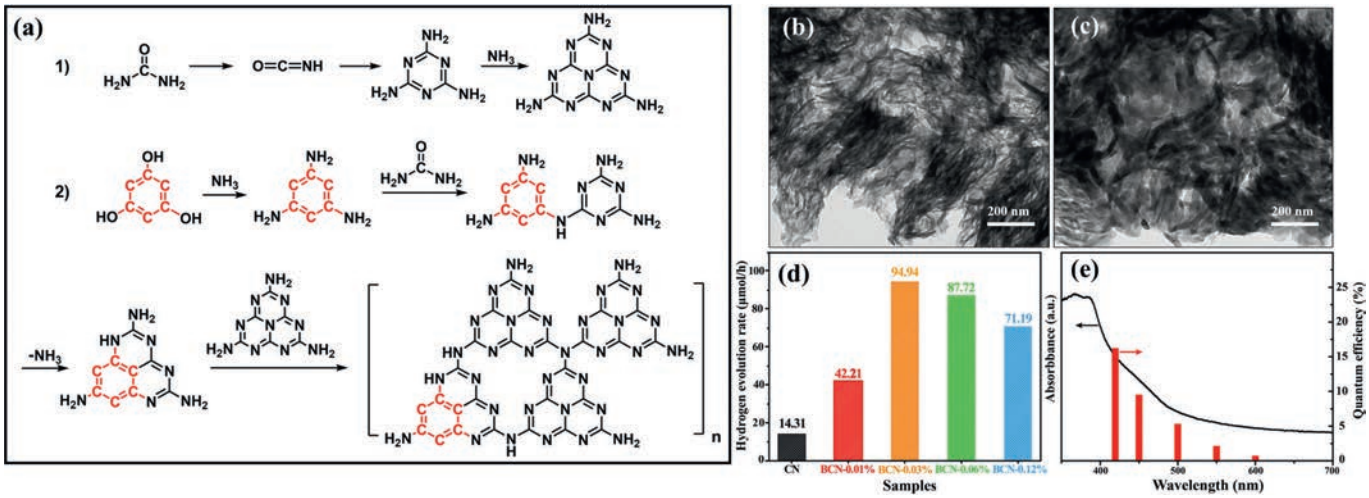

Fig. 1. (a) Schematic diagram showing the introduction of the benzene ring structure into g-C_3N_4. Typical TEM images of (b) CN and (c) BCN-0.03%. (d) Photocatalytic H_2 generation of all samples under visible light irradiation ($\lambda > 420$ nm). (e) Wavelength-dependent EQE for photocatalytic H_2 evolution over BCN-0.03%. For photocatalytic H_2 generation testing, 10 mg of photocatalyst was added in aqueous solution with 10% lactic acid as the sacrificial reagent.

selecting the dopants without the cost of structural damage in the materials.

Herein, we report a new class of g-C_3N_4 with remarkably improved π-π conjugation by rationally introducing 1,3,5-benzenetriol as a copolymer in the calcination of urea, for use as a H_2 evolution photocatalyst. The benzene ring-doped coplanar heterojunction not only retains the original structure of g-C_3N_4 but also provides an excellent driving force for facilitating charge transportation through the enhanced π-conjugated endogenous electric field. The new photocatalyst was synthesized by a thermal copolymerization strategy, shown in Fig. 1a, and labeled as BCN-*x* where *x* indicates the mol% value of 1,3,5-benzenetriol. Pure g-C_3N_4 was obtained by the same synthesis method, where $x = 0$, labelled CN. In the process of (1), urea is decomposed into ammonia and isocyanic acid at a high temperature, and then isocyanic acid polymerized into melamine [32,33]. During the process of (2), the red colored structure represents the benzene ring. At the reaction process of (2), the hydroxyl groups of 1,3,5-benzenetriol react with ammonia, while urea further reacts on the amino groups to form a cyclized in-plane heterogeneous unit [34]. Finally, these heterostructure units are further polymerized with melamine at a high temperature to form a planar heterojunction structure. Figs. 1b and c and Fig. S1 (Supporting information) show typical Transmission Electron Microscope (TEM) images of CN and BCN-0.03% samples, indicating no change in the morphology of g-C_3N_4 when 1,3,5-benzenetriol is introduced. According to the results of energy dispersive spectrometer (EDS) element analysis (Fig. S2 and Table S1 in Supporting information) and organic element analysis (Table S2 in Supporting information), with the addition of 1,3,5-benzenetriol, the atomic C/N ratio was found to increase in the material, indicating successful inclusion of the benzene ring [35]. Table S3 (Supporting information) shows the pore structure parameters and specific surface area of the CN and BCN-*x* samples, which implies that the pore size showed a downward trend, while the pore volume first increased and then decreased with the addition of more 1,3,5-benzenetriol. This can be attributed to the relative inhibitory effect of the benzene ring on the polymerization of the triazine ring, which causes the distortion of the g-C_3N_4 plane structure [22]. Appropriate distortion is conducive to the increase of pores, but severe distortion causes the instability of the g-C_3N_4 structure, causing some large pores to collapse [22,35]. Among all the samples, the BCN-0.03% sample shows the largest specific surface area, which means that the photocatalyst exposes more active sites and the shorter electron diffusion path, thus improving the photocatalytic activity. In Fig. 1d and Fig. S3 (Supporting information), it can be seen that the introduction of a small amount of benzene ring structure greatly increases the photocatalytic hydrogen evolution performance of g-C_3N_4 material. The BCN-0.03% sample showed the highest hydrogen evolution performance, reaching 94.94 μmol/h with the external quantum efficiency (EQE) of 16.4% at 420 nm (Fig. 1e), a 6.6 fold increase over that of the undoped CN. Moreover, after 16 h of photocatalytic reaction, the hydrogen evolution performance of the BCN-0.03% and the CN did not show apparent change, demonstrating the high stability of the samples (Fig. S4 in Supporting information).

Figs. S5 and S6 (Supporting information) show the X-ray diffraction (XRD) patterns and Fourier transform infrared spectroscopy (FT-IR) of CN and BCN-*x* samples. The characteristic peaks in the XRD and FT-IR spectra correspond to the classic peaks of g-C_3N_4, and the intensity of the XRD peaks remained the same, indicating that the basic g-C_3N_4 structure was preserved in the samples, preserving the crystallinity after introducing the benzene ring structure. To further elucidate the changes in the chemical structure of g-C_3N_4 caused by introducing the benzene ring, we also performed X-ray photoelectron spectroscopy (XPS) analysis (Fig. S7 in Supporting information) and solid-state ^{13}C nuclear magnetic resonance (NMR) analysis. Fig. S8 (Supporting information) displays the N 1s XPS spectra and constituent peaks of CN and BCN-0.03% sample [36]. As shown in the synthesis scheme, the introduction of the benzene ring structure replaced the position of a triazine ring unit in the tri-*s*-triazine ring, thereby changing the C/N ratio in the samples and also the ratio of nitrogen in different chemical environments (Table S4 in Supporting information) [27,37]. Fig. 2a shows the ^{13}C NMR spectra of CN, BCN-0.03% and BCN-0.12% sample. The spectra show two main resonance peaks at 164.2 and 156.1 ppm, corresponding to C(1) atoms and C(2) atoms in tri-*s*-triazine rings, respectively [34]. It should be noted that the BCN-0.12% spectrum exhibits an additional weak and broad peak at 132.1 ppm, which is ascribed to the emergence of aromatic rings [37], while the peak of BCN-0.03% did not appear due to the low doping concentration. The XPS and NMR results are both consistent with the above conclusion, which further proves that the benzene ring structure was successfully introduced into the network structure of g-C_3N_4, and subsequently constructed an enhanced π-π conjugation structure.

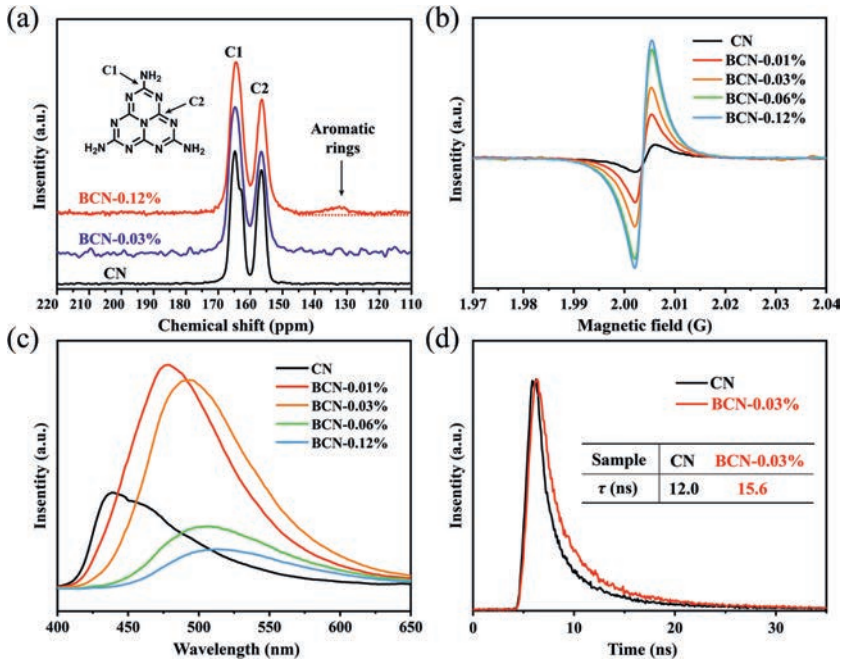

Fig. 2. (a) Solid-state ^{13}C NMR spectra of the CN and BCN-0.12% samples. (b) Room-temperature EPR spectra of all samples. (c) PL spectra of all samples. (d) Transient state photoluminescence spectra of CN and BCN-0.03% samples.

Fig. S9a (Supporting information) shows the ultraviolet visible (UV-vis) diffuse reflectance spectra of CN and BCN-*x* samples. As the amount of benzene ring increases, the maximum absorption edge was significantly broadened, which indicated that introduction of the benzene ring enlarges the delocalization range of the electrons in g-C_3N_4. Furthermore, the external quantum efficiency (Fig. 1e), measured at 420, 450, 500, 550 and 600 nm, matched well with the absorption value of the sample. Tauc plots were generated to estimate the optical band gap of the prepared samples [38,39], shown in Fig. S9b (Supporting information). Electron paramagnetic resonance (EPR) tests were performed, shown in Fig. 2b, indicating the degree of electron delocalization of the samples. The spectra exhibit a single peak with a g-value of 2.003 [40], which was attributed to the unpaired electrons of the g-C_3N_4 networks within π-bonded clusters. Compared with CN, BCN-*x* samples have a stronger EPR signal, indicating that the incorporation of benzene ring significantly extended the π-conjugated system and enhanced the electron delocalization, which reduced the resistance of electron transportation, leading to the observed increase in photocatalytic activity.

It is of importance to understand the influence of the new π-π conjugation structure on the electronic separation and transportation properties of the g-C_3N_4. Steady state photoluminescence (PL) spectra (Fig. 2c) showed a significant increase in PL intensity for low dopant concentration samples before decreasing as the amount of dopant increased, with all samples showing a trend of increasing red-shift as the degree of π-π conjugation increases [41,42]. The increase in PL intensity was attributed to the extension of the π-conjugation system in the g-C_3N_4, enhancing the π electron delocalization, and the observed subsequent decrease is explained by the benzene ring dopant possibly acting as a charge-trapping site, prohibiting radiative recombination, which in turn greatly enhances the separation ability of photogenerated carriers [43]. In the PL spectra, it can be observed that there were two PL emission centers of CN sample, one emission center was located at 435 nm, and the other emission center was located at 468 nm. The emission peak located at 435 nm was caused by the transition between lone pair (LP) state to δ^* antibonding state, while the emission peak at 468 nm was caused by the transition between LP state to π^* antibonding state [44,45]. As the π-conjugation degree of the BCN-*x* sample increased, the delocalization of electrons will increase, and the π^* antibonding state and the δ^* antibonding state will overlap more strongly. Hence, the probability for the excited electrons located at δ^* antibonding state relaxing to the π^* antibonding state was increasing. As a result, the $\pi^* \rightarrow$ LP emission gradually dominated the carbon nitride PL emission as the π conjugation degree of the BCN-*x* sample increases. CN and BCN-0.03% samples were selected for time-resolved fluorescence decay spectroscopy (Fig. 2d and Table S5 in Supporting information), and showed that the average lifetime of 12.0 ns in CN increased to 15.6 ns in BCN-0.03%, indicating the charge carriers of the BCN-0.03% sample have a longer lifetime.

This remarkable ability to separate photogenerated carriers is further confirmed by electrochemical testing. Transient photocurrent and electrochemical impedance spectroscopy tests were performed on BCN-0.03% and CN samples (Fig. 3a), which showed that the photocurrent obtained in the electrode of BCN-0.03% is higher than that obtained in CN, indicating an enhanced interface electron transfer resulting from benzene ring doping. The electrochemical impedance spectroscopy (Fig. 3b) shows a smaller semicircle Nyquist plot, demonstrating the lower charge transfer resistance of the BCN-0.03%. This result proves that the enhanced π-π conjugation structure can significantly reduce the migration resistance of photogenerated carriers, thereby improving the lifetime of the carriers. In order to investigate the effect of benzene ring doping on the band structure of g-C_3N_4, the Mott-Schottky test (Figs. 3c and d) and ultraviolet photoelectron spectroscopy (UPS) test (Fig. S10 in Supporting information) was performed on CN and BCN-0.03%. According to Mott-Schottky test, it can be determined that the conduction band edges of CN and BCN-0.03% are −1.30 V and −1.04 V *vs.* NHE (pH 7), respectively.

To better understand the relationship between benzene ring doping and band gap in depth, the theoretical calculations of energy and electronic structure were performed using Vienna *ab-initio* simulation package (VASP). The results model used in the calculation is shown in Schemes 1a and b. From the results of

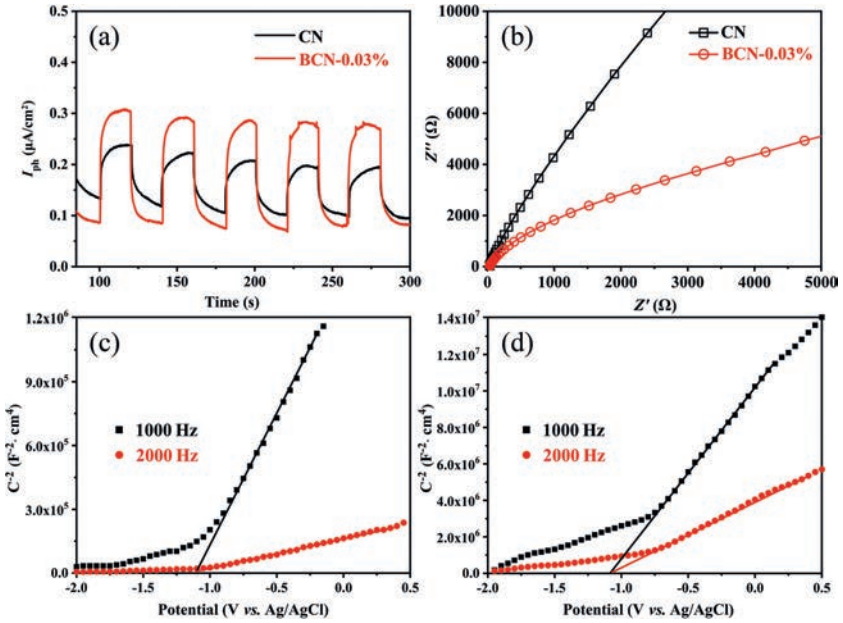

Fig. 3. (a) Photocurrent density curves of CN and BCN-0.03%. (b) EIS Nyquist plots of CN and BCN-0.03% electrodes. Mot-Schottky plots of (c) CN and (d) BCN-0.03%.

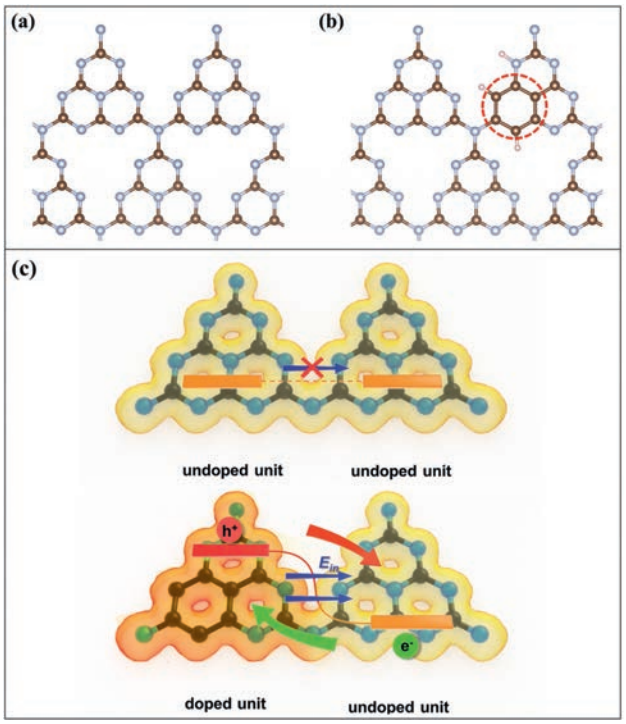

Scheme 1. Structure of (a) g-C_3N_4 and (b) benzene doped g-C_3N_4 (equivalent substitution sites circled by dashed line). (c) Schematic diagram of directional transportation of photogenerated carriers on the BCN-*x* plane.

structure optimization, there is no distortion of the g-C_3N_4 network plane in BCN structure, which is consistent with the conclusion that the crystallinity was not altered after introduction of the benzene ring, and no defects were introduced as a result of the doping. It can be clearly seen (Fig. 4a) that the electron densities of states (DOS) of CN and BCN-*x* both exhibit semiconductor properties. To further clarify the effect of the benzene ring on the band structure, the DOS diagram is divided into contributions of π and δ electron orbitals. The band gap of BCN-*x* is significantly reduced due to the π orbital contribution at the conduction band, corroborating the results of the Mot-Schottky plots. Based on the results of the Mot-Schottky and UV-vis diffuse reflectance, a schematic diagram of the band gap structure of CN and BCN-0.03% is shown in Fig. 4b. The introduction of the benzene ring in the tri-*s*-triazine units will inevitably affect the electronic localization and electrostatic potential of the g-C_3N_4 network, thereby affecting the directional transportation of electrons. Fig. S11 (Supporting information) and Figs. 4c and d show the calculation results of electron localization function (ELF) and electrostatic potentials of CN and BCN-*x* samples, respectively. According to the calculation results of the electrostatic potential of CN and BCN-*x*, the work functions are 4.15 eV and 3.94 eV, respectively, suggesting that the benzene ring will increase the electrostatic potential of the tri-*s*-triazine units. The electrons, therefore, would spontaneously transfer through the benzene ring doped tri-*s*-triazine units to the undoped units until their Fermi levels are the same, resulting in a net loss of electron density, and a concomitant increase in electron density in the undoped units, thus generating an endogenous directional electric field in the planar network structure.

According to the above results, Scheme 1c shows the electric field inside the CN and BCN-*x* material. In Scheme 1c, the color of the electron cloud outside the g-C_3N_4 structure indicates the degree of delocalization, and the blue arrow indicates the direction of the electric field in the planar structure. Since the pristine g-C_3N_4 has the same tri-*s*-triazine units, there is no such endogenous directional electric field, thus no driving force for photogenerated electrons, which makes it difficult to migrate to the photocatalyst surface thereby recombining inside the bulk material. In contrast, in the structure of BCN-*x*, driven by the electric field, photogenerated electrons move to the benzene ring doped tri-*s*-triazine units (indicated by green arrow in Scheme 1c), which act as charge-trapping sites, limiting the recombination of the photogenerated charge carriers, consistent with the PL results. On the other side, photogenerated holes migrate to the opposite direction under visible light irradiation driven by the endogenous electric field (red arrow in Fig. 1c), thereby significantly reducing carrier recombination, allowing more charges to participate in the hydrogen evolution reaction, and greatly improving the activity.

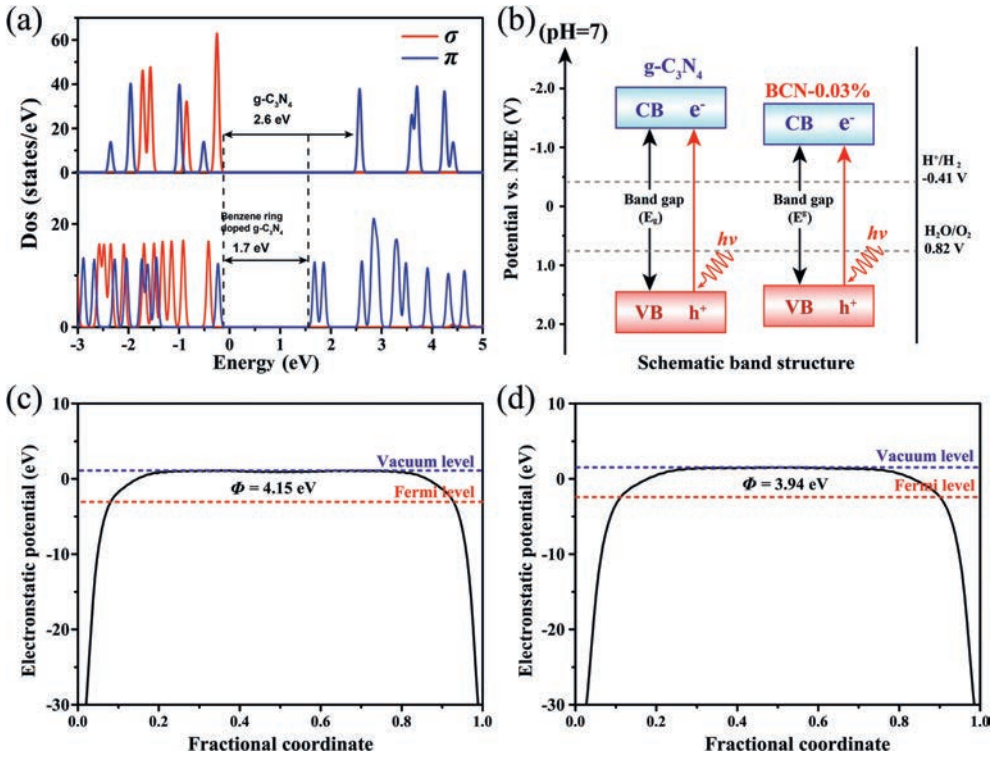

Fig. 4. (a) DOSs for CN and BCN-*x*. (b) Band gap structure diagram for g-C_3N_4 and BCN-0.03%. Electrostatic potentials of (c) CN surface and (d) BCN surface.

In summary, a unique coplanar heterostructure in the π-conjugated g-C_3N_4 photocatalysts was successfully generated by selective doping the g-C_3N_4 during a simple calcination process. The dopant, 1,3,5-benzenetriol, can easily participate in the formation of a tri-*s*-triazine unit and ensure the integrity of the pristine network structure of carbon nitride, thereby forming a coplanar heterojunction via enhanced π-π conjugation. This new structure can significantly expand the light absorption range of g-C_3N_4 and increase the separation and transportation rate of photogenerated carriers. The photoelectrochemical characterization and theoretical calculation results show that the decrease of the BCN-*x* band gap is mainly due to the contribution of the π electron orbit. In addition, the transportation of photogenerated carriers was further calculated by the work function, indicating that photogenerated electrons transfer to the benzene ring doped units and photogenerated holes transfers to the undoped units, thereby significantly reducing charge carrier recombination. This finding proposes a new design principle which can be applied to other two-dimensional organic photocatalysts to achieve a higher solar energy conversion efficiency

Declaration of competing interests

The authors declare that they have no known competing financial interests or personal relationships that could have appeared to influence the work reported in this paper.

Acknowledgments

This work was financially supported by the National Natural Science Foundation of China (Nos. U1862105, 22078256), Natural Science Basic Research Plan in Shaanxi Province of China (Nos. 2017JZ001, 2018KJXX-008), Fundamental Research Funds for the Central Universities (No. cxtd2017004) and K.C. Wong Education Foundation, Hong Kong, China, and financial support from Australian Research Council are appreciated.

Supplementary materials

Supplementary material associated with this article can be found, in the online version, at doi:10.1016/j.cclet.2021.08.118.

References

[1] J. Liu, Y. Liu, N. Liu, et al., Science 347 (2015) 970–974.
[2] X. Chen, S. Shen, L. Guo, et al., Chem. Rev. 110 (2010) 6503–6570.
[3] S. Chen, T. Takata, K. Domen, Nat. Rev. Mater. 2 (2017) 17050.
[4] B. Lin, G. Yang, L. Wang, Angew. Chem. Int. Ed. 58 (2019) 4587–4591.
[5] B. Zhu, L. Zhang, B. Cheng, et al., Chin. J. Catal. 42 (2021) 115–122.
[6] Y. Xing, X. Wang, S. Hao, et al., Chin. Chem. Lett. 32 (2021) 13–20.
[7] B. Lin, H. Chen, Y. Zhou, et al., Chin. Chem. Lett. 32 (2021) 3128–3132.
[8] B. Lin, B. Ma, J. Chen, et al., Chin. Chem. Lett. 33 (2022) 943–947.
[9] H. Li, H. An, B. Chong, G. Yang, L. Wang, Chem. Eng. Sci. 238 (2021) 116594.
[10] W. Wang, M. Chen, D. Huang, et al., Compos. Part B: Eng. 172 (2019) 704–723.
[11] M. Yu, H. Liang, R. Zhan, et al., Chin. Chem. Lett. 32 (2021) 2155–2158.
[12] B. Lin, Z. Chen, P. Song, et al., Small 16 (2020) 2003302.
[13] B. Lin, A. Chaturvedi, J. Di, et al., Nano Energy 76 (2020) 104972.
[14] Z. Tang, C. Wang, W. He, et al., Chin. Chem. Lett. 33 (2022) 939–942.
[15] Y. Ishida, L. Chabanne, M. Antonietti, et al., Langmuir 30 (2014) 447–451.
[16] J. Zhang, G. Zhang, X. Chen, et al., Angew. Chem. Int. Ed. 51 (2012) 3183–3187.
[17] C. Wang, H. Dong, L. Jiang, et al., Chem. Soc. Rev. 47 (2018) 422–500.
[18] Y. Gong, J. Lin, X. Wang, et al., Nat. Mater. 13 (2014) 1135–1142.
[19] B. Zhu, L. Zhang, B. Cheng, et al., Appl. Catal. B: Environ. 224 (2018) 983–999.
[20] W. Zheng, N.-B. Wong, G. Zhou, et al., New J. Chem. 28 (2004) 275–283.
[21] W. Ho, Z. Zhang, W. Lin, et al., ACS Appl. Mater. Interfaces 7 (2015) 5497–5505.
[22] X. Fan, L. Zhang, R. Cheng, et al., ACS Catal. 5 (2015) 5008–5015.
[23] J. Liu, Y. Yu, R. Qi, et al., Appl. Catal. B: Environ. 244 (2019) 459–464.
[24] J. Qin, S. Wang, H. Ren, et al., Appl. Catal. B: Environ. 179 (2015) 1–8.
[25] S. Bai, X. Li, Q. Kong, et al., Adv. Mater. 27 (2015) 3444–3452.
[26] S. Bai, J. Ge, L. Wang, et al., Adv. Mater. 26 (2014) 5689–5695.
[27] P.K. Chuang, K.H. Wu, T.F. Yeh, et al., ACS Sustain. Chem. Eng. 4 (2016) 5989–5997.
[28] W. Xing, W. Tu, Z. Han, et al., ACS Energy Lett. 3 (2018) 514–519.
[29] Y. Cui, G. Zhang, Z. Lin, et al., Appl. Catal. B: Environ. 181 (2016) 413–419.
[30] L. Lin, Z. Yu, X. Wang, Angew. Chem. Int. Ed. 58 (2019) 6164–6175.
[31] M. Shalom, S. Inal, C. Fettkenhauer, et al., J. Am. Chem. Soc. 135 (2013) 7118–7121.
[32] A.M. Bernhard, D. Peitz, M. Elsener, et al., Appl. Catal. B: Environ. 115 (2012) 129–137.
[33] D. Mitoraj, H. Kisch, Chem. Eur. J. 16 (2010) 261–269.
[34] B. Jürgens, E. Irran, J. Senker, et al., J. Am. Chem. Soc. 125 (2003) 10288–10300.
[35] J. Li, D. Wu, J. Iocozzia, et al., Angew. Chem. Int. Ed. 58 (2019) 1985–1989.

[36] A. Thomas, A. Fischer, F. Goettmann, et al., J. Mater. Chem. 18 (2008) 4893–4908.
[37] H. Kim, S. Gim, T.H. Jeon, et al., ACS Appl. Mater. Interfaces 9 (2017) 40360–40368.
[38] H. Wang, X. Zhang, J. Xie, et al., Nanoscale 7 (2015) 5152–5156.
[39] H. Li, N. Wells, B. Chong, et al., Chem. Eng. Sci. 229 (2021) 116069.
[40] Y. Li, D. Zhang, J. Fan, et al., Chin. J. Catal. 42 (2021) 627–636.
[41] Z. Zhang, Y. Zhang, D. Yao, et al., Cryst. Growth Des. 9 (2009) 5069–5076.
[42] Y. Ooyama, T. Nakamura, K. Yoshida, New J. Chem. 29 (2005) 447–456.
[43] H. Wang, X. Sun, D. Li, et al., J. Am. Chem. Soc. 139 (2017) 2468–2473.
[44] Y. Zhang, Q. Pan, G. Chai, et al., Sci. Rep. 3 (2013) 1943.
[45] Z. Gan, Y. Shan, J. Chen, et al., Nano Res. 9 (2016) 1801–1812.